Cell

Crystal Structures of *T. brucei* MRP1/MRP2 Guide-RNA Binding Complex Reveal RNA Matchmaking Mechanism

Maria A. Schumacher,[1,*] Elham Karamooz,[1,3] Alena Zíková,[2,4] Lukáš Trantírek,[2] and Julius Lukeš[2]
[1] Department of Biochemistry and Molecular Biology, University of Texas, M.D. Anderson Cancer Center, Unit 1000, Houston, TX 77030, USA
[2] Biology Centre, Institute of Parasitology, Czech Academy of Sciences and Faculty of Biology, University of South Bohemia, Branišovská 31, 37005 České Budějovice (Budweis), Czech Republic
[3] University of Illinois College of Medicine, 190 Medical Sciences Building, MC-714, 506 South Mathews Avenue, Urbana, IL 61801, USA
[4] Seattle Biomedical Research Institute, 307 Westlake Avenue, Seattle, WA 98103, USA
*Contact: maschuma@mdanderson.org
DOI 10.1016/j.cell.2006.06.047

SUMMARY

The mitochondrial RNA binding proteins MRP1 and MRP2 form a heteromeric complex that functions in kinetoplastid RNA editing. In this process, MRP1/MRP2 serves as a matchmaker by binding to guide RNAs and facilitating their hybridization with cognate preedited mRNAs. To understand the mechanism by which this complex performs RNA matchmaking, we determined structures of *Trypanosoma brucei* apoMRP1/MRP2 and an MRP1/MRP2-gRNA complex. The structures show that MRP1/MRP2 is a heterotetramer and, despite little sequence homology, each MRP subunit exhibits the same "Whirly" transcription-factor fold. The gRNA molecule binds to the highly basic β sheet surface of the MRP complex via nonspecific, electrostatic contacts. Strikingly, while the gRNA stem/loop II base is anchored to the basic surface, stem/loop I (the anchor sequence) is unfolded and its bases exposed to solvent. Thus, MRP1/MRP2 acts as an RNA matchmaker by stabilizing the RNA molecule in an unfolded conformation suitable for RNA-RNA hybridization.

INTRODUCTION

The trypanosomatids represent a major group of parasitic protozoans within the kinetoplastid flagellates, which include the pathogenic species from the genera *Leishmania* and *Trypanosoma* that are the causative agents of leishmaniases, African sleeping sickness, and Chagas disease (Simpson et al., 2006). Studies on these early diverging eukaryotes have revealed a plethora of novel biological processes, perhaps the most remarkable of which is kinetoplastid RNA editing (kRNA editing), which occurs in the mitochondrion (Benne et al., 1986; Feagin et al., 1988a; Shaw et al., 1988; Horváth et al., 2000). kRNA editing is a highly complex process that involves the insertion and/or deletion of uridine (U) nucleotides in the coding regions of at least 12 of the 18 *Trypanosoma brucei* mitochondrial mRNAs. These insertion/deletion events generate start codons, correct frameshifts, and even create entire open reading frames (Madison-Antenucci and Hajduk, 2002; Simpson et al., 2003, 2004; Stuart et al., 2005; Lukeš et al., 2005). Its extreme form, termed pan-editing, is exemplified by formation of the cytochrome c oxidase III mRNA, in which 547 Us are inserted and 41 Us are deleted to produce the mature transcript (Feagin et al., 1988b). The kRNA editing process is directed by a large number of small RNAs, termed guide RNAs (gRNAs), most of which are transcribed from kDNA minicircles (Blum et al., 1990; Sturm and Simpson, 1990). In *T. brucei*, about 10,000 minicircles, concatenated into a single huge network (Liu et al., 2005; Lukeš et al., 2005), encode an estimated number of ~150 gRNAs (Hong and Simpson, 2003). These gRNAs, which are typically 50–70 nucleotides long, are essential to kRNA editing as they contain the sequence information required by the editing machinery to dictate the correct insertion and/or deletion of Us at precise locations in the pre-mRNA (Corell et al., 1993; Seiwert and Stuart, 1994).

Structure-sensitive chemical and enzymatic probes along with spectroscopic analyses demonstrated that gRNA molecules, although distinct in their sequences, have a conserved secondary structure, consisting of three key elements: two stem/loop (hairpin loop) regions, named stem/loop I and II, and a 3′ oligo(U)-tail (Schmid et al., 1995; Hermann et al., 1997). The most 5′ sequence contains stem/loop I and is called the "anchor sequence," which is complementary to the mRNA just 3′ of the first

editing site and thus specifies the interaction between the gRNA and its cognate mRNA. The central portion of the gRNA, stem/loop II, encodes the editing information and is complementary to the resulting edited mRNA. The 3′ end of each gRNA contains an oligo(U)-tail and, although its function is unknown, it has been postulated that it interacts with the purine-rich region upstream of the editing site to help stabilize the complex (Blum et al., 1990; Seiwert et al., 1996). Biochemical data have clearly demonstrated that the two stem/loops of gRNAs have low stability thermodynamically. This finding suggests that gRNA molecules are fine tuned to minimize their structural stability to permit the annealing reaction with pre-mRNA while at the same time maximizing higher-order structural features that mediate specific recognition and assembly with editing factors (Blum and Simpson, 1990).

The process of kRNA editing appears to take place in a series of cut-and-paste steps and is carried out by a still incompletely characterized supramolecular complex, the L-complex (for Ligase-containing complex), which consists of ~16–20 proteins and contains stoichiometric amounts of the four key enzymatic core activities: an editing endonuclease, a terminal uridylyl transferase (TUTase), an RNA ligase, and an exonuclease (Corell et al., 1996; Panigrahi et al., 2001, 2003; Aphasizhev et al., 2003a; Simpson et al., 2004). Editing proceeds from 3′ to 5′ both within a single gRNA-mediated block and also within the entire editing domain. This latter 3′ to 5′ polarity is caused by the creation of new anchor sequences by the downstream gRNA for hybridization of the adjacent upstream gRNA (Maslov and Simpson, 1992). The current model of kRNA editing proposes that the gRNA first hybridizes downstream of the first editing site via its anchor sequence (stem/loop I). Next, the endonuclease cleaves at a mismatched base and TUTase adds U nucleotides to the 3′ end of the 5′ cleavage product. The added Us can then base-pair with the guiding nucleotides in the gRNA and extend the duplex. The nonbase-paired Us are trimmed by an exonuclease, and an RNA ligase joins the modified fragments. The editing machinery then advances to the next upstream site.

In addition to the critical core enzymes, the L complex contains substoichiometric amounts of RNA-linked proteins that are essential for in vivo editing. One protein complex is the MRP complex (*m*itochondrial *R*NA binding *p*rotein complex), which is composed of two subunits, MRP1 and MRP2 (Aphasizhev et al., 2003b; Simpson et al., 2004; Vondrušková et al., 2005). MRP1 was originally identified as an arginine-rich factor in *T. brucei* that specifically crosslinks to gRNAs, and homologs were later identified in *Leishmania tarentolae* and *Crithidia fasciculata* (Köller et al., 1997; Blom et al., 2001; Müller et al., 2001; Müller and Göringer, 2002; Aphasizhev et al., 2003b). Subsequently, it was shown that in all these flagellates, MRP1 interacts with a second protein, MRP2, to form a complex and that both proteins have a mutual dependence for stability (Vondrušková et al., 2005). Interestingly, although the MRPs bind gRNAs with nM affinity, studies suggested that this binding is largely electrostatic and nonsequence specific (Köller et al., 1997; Müller and Göringer, 2002; Aphasizhev et al., 2003b). Data showing that the MRP-gRNA complex are extremely salt sensitive supports this idea (Köller et al., 1997). However, there are conflicting reports as to the ability of the MRPs to bind single-stranded RNA (ssRNA) and/or double-stranded RNA (dsRNA), and thus the binding mode utilized by the MRPs to interact with RNA is not clear (Köller et al., 1997; Müller and Göringer, 2002; Aphasizhev et al., 2003b). Because the MRPs were identified based on their specific crosslinking with gRNAs, it was proposed initially that they function in the initial stages of editing, particularly in the formation of the gRNA-pre-mRNA duplexes (Lambert et al., 1999; Müller et al., 2001). Subsequent studies revealed the pivotal finding that MRPs not only bind gRNAs but also somehow function in matchmaking by promoting the annealing of the gRNAs to their cognate pre-mRNAs (Müller and Göringer, 2002; Aphasizhev et al., 2003b). The MRPs show no sequence homology to any other protein; thus the structure of the MRP1/MRP2 complex and how it recognizes gRNAs and facilitates the gRNA-pre-mRNA annealing reaction is unknown. To address these questions, we carried out a detailed analysis of RNA binding by MRP1/MRP2 and determined crystal structures of the *T. brucei* apoMRP1/MRP2 complex and an MRP1/MRP2-gRNA complex.

RESULTS AND DISCUSSION

Overall Structure of the apoMRP1/MRP2 Complex

To obtain the MRP1/MRP2 complex, the DNA fragments encoding mature MRP1 and MRP2 proteins, i.e., minus the mito-targeting sequences, were subcloned into the pETDuet-1 system for coexpression (see Experimental Procedures). The purified complex was crystallized and the structure solved by Multiple Wavelength Anomalous Dispersion (MAD) (Figure 1A; Table 1). There are two MRP1 and two MRP2 molecules in the crystallographic asymmetric unit (ASU) and the final structure includes residues 28–173 of both MRP1 subunits, residues 55–175 and 188–221 of one MRP2 subunit, residues 56–175 and 188–221 of the second MRP2 subunit, 8 acetate molecules, and 572 water molecules. The final refined structure has an R_{free} of 21.7% to 1.89 Å resolution (Table 1).

MRP1 and MRP2 Share a Similar Fold and Form a Heterotetramer

The MRP1/MRP2 structure reveals that both the fold exhibited by MRP1 and MRP2 and the oligomeric arrangement of the complex are distinct from structures of RNA binding proteins that have been characterized to date (Nagai, 1996). Specifically, MRP1 and MRP2 combine to form a heterotetramer with pseudocyclic C4 symmetry (Figure 1B). The strong pseudosymmetry results from the finding that the folds of MRP1 and MRP2 are remarkably similar, despite the fact that the proteins display only 18% sequence identity. Indeed, 126 corresponding Cα atoms

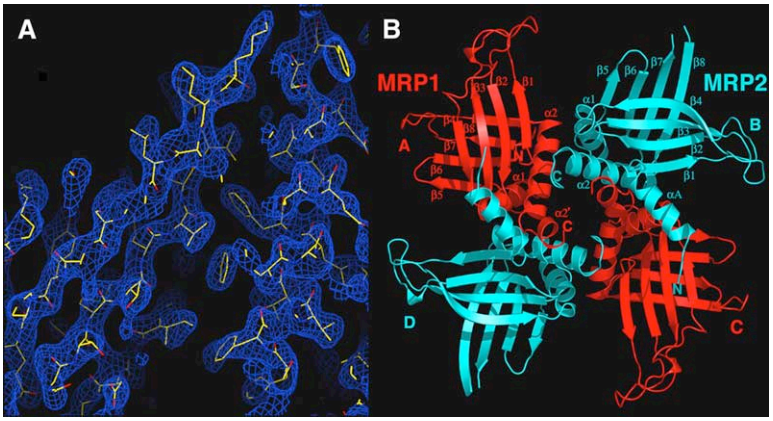

Figure 1. Structure of the MRP1/MRP2 Complex

(A) Experimental 2.4 Å MAD electron density map (blue mesh) of the MRP1/MRP2 complex contoured at 1.2 σ. The proteins are shown as sticks with nitrogen, oxygen, carbon, and sulfur atoms colored blue, red, yellow, and green, respectively. This figure and Figures 4A and 4B were made using O (Jones et al., 1991).

(B) Ribbon diagram of the apoMRP1/MRP2 complex. MRP1 is colored red, and MRP2 is cyan. The secondary structure elements and N and C termini of one subunit of MRP1 and MRP2 are labeled. This figure and Figures 2A, 5A, and 6B–D were made with PyMOL (Delano, 2002).

of MRP1 can be optimally superimposed onto those of MRP2 with a root mean-squared deviation (RMSD) of only 1.38 Å (Figures 2A and 2B). MRP1 and MRP2 share an overall conserved β-β-β-β-α-β-β-β-β-α topology, and each of the four β strands within a given β-β-β-β-α repeat form a curved antiparallel β sheet that packs perpendicularly against the β sheet from the other repeat. The topologies of MRP1 and MRP2 differ mainly in that MRP1 has a bent α2 helix while MRP2 has an extra α helix at its N-terminal region, termed αA (Figures 2A and 2B). The topological arrangement of MRP1 is β-β-β-β-α-β-β-β-β-α-α′ (β1: residues 30–38, β2: 44–52, β3:55–62, β4:83–89, α1:90–101, β5:104–111, β6:114–120, β7:124–131, β8:139–147, α2:148–165 and α2′:167–173) and of MRP2 is α-β-β-β-β-α-β-β-β-β-α (αA: 63–70, β1:73–81, β2:88–96, β3:99–107, β4:117–126, α1:128–138, β5:144–148, β6:152–157, β7:166–173, β8:190–197, α2:198–218).

The β sheets of each MRP β-β-β-β-α repeat form blade-like extensions that emanate from the circular α-helical core of the heterotetramer (Figure 1B). The main oligomerization contacts are mediated by these α helices, which assemble near the center of the tetramer. The surface area buried by formation of the A:D (and B:C) dimer is an extensive 2300 Å^2 while the A:B (and D:C) dimer interface buries 1443 Å^2. Both dimer interfaces are primarily hydrophobic and contain a large number of aromatic residues that participate in stacking interactions. The large buried surface area of the MRP oligomerization interfaces and the significant number of hydrophobic contributions to these interfaces is consistent with the finding that MRP1 and MRP2 must oligomerize to be stable (A.Z., K.S., and J.L.; unpublished data). A second MRP1/MRP2 crystal form (solved to 3.35 Å resolution) and grown under different conditions from our first crystal form revealed two crystallographically independent MRP1/MRP2 heterotetramers that are identical to the 1.89 Å MRP1/MRP2 heterotetramer structure. Additional studies support the contention that the heterotetramer is the functional form of the MRP1/MRP2 complex in other trypanosomatids. For example, immunoprecipitation experiments revealed clear interactions between the MRP homologs from *C. fasciculata*, gBP29 and gBP27, and the MRP homologs from *L. tarentolae*, Ltp26 and Ltp28, were shown to form a 100 kDa complex that contains two copies each of Ltp26 and Ltp28, consistent with a heterotetramer (Aphasizhev et al., 2003b; Blom et al., 2001).

The MRPs: A New Class of RNA Binding Proteins with a Plant-like "Whirly" Heterotetramer Fold

To identify proteins with structural homology to the MRP fold and/or the MRP1/MRP2 heterotetramer, we carried out structural comparison searches (Holm and Sander, 1995). These homology searches revealed a striking structural correspondence between the MRPs and only one protein, the plant ssDNA binding transcription factor p24 (Desveaux et al., 2002). The structural homology between the MRPs and p24 is not only striking in that the protomer folds of these proteins are extremely similar but also the oligomeric architecture of these proteins is analogous except that p24 is a homotetramer. Indeed, the whirligig appearance of the tetrameric p24 structure led to the designation of this family of plant transcription factors as the "Whirly" proteins (Desveaux et al., 2002). The individual subunits of MRP1 and MRP2 superimpose onto that of p24 with RMSDs of 1.98 Å and 1.64 Å for 105 and 107 similar Cα atoms, respectively, and the MRP1/MRP2 heterotetramer optimally superimposes onto the p24 homotetramer with an RMSD of 2.22 Å for 262 corresponding Cα atoms. The structural homology between the MRPs and p24 is particularly striking in light of the fact that there is essentially no sequence homology between these proteins. This similarity is also interesting in light of recent studies demonstrating that the p24 homologs are targeted to plant organelles, including the mitochondrion, and that the plant "Whirly" proteins may also form heterotetramers (Krause et al., 2005).

Biochemical Characterization of the Interaction of *T. brucei* MRP1/MRP2 with RNA

The MRP proteins were isolated as components specifically crosslinked to gRNAs and have been shown to be essential for in vivo kRNA editing; however, studies examining the RNA binding properties of these proteins have provided results that are equivocal (Köller et al., 1997;

Table 1. Selected Crystallographic Data for MRP Complexes

Wavelength (λ)	1.00640	1.00840	0.99180
Resolution (Å)	58.72–2.35	58.72–2.35	58.72–2.35
overall R_{sym} (%)[a]	6.2 (29.0)[b]	6.2 (29.5)	6.2 (29.5)
overall I/σ (I)	7.7 (2.5)	7.7 (2.3)	7.8 (2.3)
# Total Reflections	181835	181835	181835
# Unique Reflections	34161	34160	34160
Multiplicity	5.3	5.4	5.4
Overall Figure of Merit[c]			0.590
Crystal form	MRP1/MRP2 (apoI)	MRP1/MRP2 (apoII)	MRP1/MRP2-gRNA
Space Group	$P2_1$	R3	$P6_122$
Cell Parameters (Å)	a = 60.3, b = 85.7	a = b = 236.0	a = b = 157.6
	C = 86.9, b = 109.4°	c = 85.4	c = 81.3
Resolution (Å)	58.72–1.89	79.06–3.35	81.65–3.37
Overall R_{sym}(%)[a]	4.8 (35.9)	11.8 (51.4)	12.7 (48.5)
Overall I/σ (I)	10.5 (2.2)	5.7 (1.7)	5.1 (1.8)
# Total Reflections	220146	75417	22542
# Unique Reflections	63446	25300	8126
% Complete	95.3 (80.0)	99.3 (99.3)	91.9 (70.0)
Refinement Statistics			
Resolution (Å)	58.72–1.89	79.06–3.35	81.65–3.37
R_{work}/R_{free} (%)[d]	17.9/21.7	23.9/29.9	27.9/29.8
Rmsd			
Bond Angles (°)	1.65	1.58	2.09
Bond Lengths (Å)	0.014	0.009	0.013
B-values ($Å^2$)			
Average B Values ($Å^2$)	3.7	2.7	3.6

[a] $R_{sym} = \Sigma\Sigma|Ihkl-Ihkl(j)|/ \Sigma Ihkl$, where Ihkl(j) is observed intensity and Ihkl is the final average value of intensity.
[b] Values in parentheses are for the highest resolution shell.
[c] Figure of Merit = $<|\Sigma P(\alpha)e^{i\alpha}/\Sigma P(\alpha)|>$, where α is the phase and P(α) is the phase probability distribution.
[d] $R_{work} = \Sigma||F_{obs}| - |F_{calc}||/\Sigma|F_{obs}|$ and $R_{free} = \Sigma||F_{obs}| - |F_{calc}||/\Sigma|F_{obs}|$; where all reflections belong to a test set of 5% randomly selected data.

Lambert et al., 1999; Müller et al., 2001; Aphasizhev et al., 2003b). For instance, studies on *T. brucei* MRP1 indicate that it binds gRNAs and ssRNAs with high affinity but interacts with dsRNAs with ~100-fold lower affinity (Köller et al., 1997; Lambert et al., 1999; Müller et al., 2001). By contrast, studies on the *L. tarentolae* MRP complex revealed that it can be isolated from mitochondria specifically crosslinked to gRNAs but that it can also bind ssRNAs and dsRNAs with high and nearly equal affinity (Aphasizhev et al., 2003b). The apparent discrepancies between these studies could be attributed to the use of only MRP1 in the *T. brucei* studies, the different conditions under which the binding was carried out, and/or species variation. However, one shared conclusion from these analyses is that the MRPs appear to show little or no sequence specificity in RNA binding (Köller et al., 1997; Lambert et al., 1999; Müller et al., 2001). Thus, to provide a detailed description of RNA binding by the *T. brucei* MRP1/MRP2 complex, including its gRNA binding properties, we employed a fluorescence polarization (FP) binding assay. We first tested the ability of MRP1/MRP2 to bind RNA fragments based on the gRNA, gND7-506 (Figure 3A). gND7-506 is a gRNA that directs the editing of a sequence domain near the 5′ end of the mRNA for subunit 7 of NADH dehydrogenase (ND7) (Koslowsky et al., 1992). Importantly, multiple analyses have confirmed that gND7-506 adopts the archetypical gRNA secondary structure with two stem/loops and a 3′ oligo(U)-tail (Hermann et al., 1997; Müller et al., 2001). We found that the MRP1/MRP2 complex binds the stem/loop II (oligo I) and

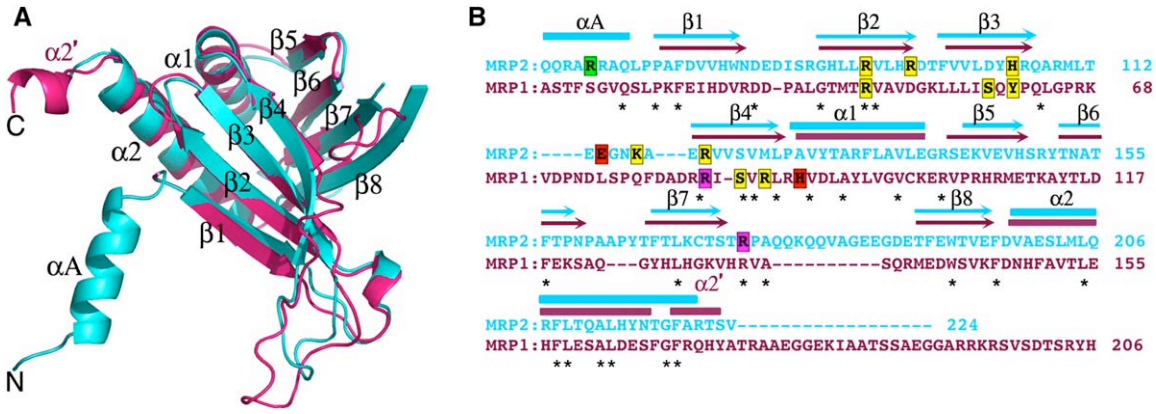

Figure 2. MRP1 and MRP2 Have "Whirly" Transcription-Factor Folds and Form a Heterotetramer

(A) Optimized superimposition of one MRP1 subunit (pink) onto one MRP2 subunit (cyan).

(B) Structure-ased sequence alignment of MRP1 (pink) and MRP2 (cyan). Secondary structural elements are shown above the sequence colored according to the protein they represent. Helices are represented as solid tubes and β trands, by arrows. Sequence identities between the MRPs are indicated by asterisks. Boxed and colored are residues that interact with the gRNA in the MRP1/MRP2-gRNA structure. Residues boxed in yellow, green, red, and magenta participate in phosphate contacts, ribose 2′hydroxyl contacts, nonspecific base contacts and interactions with both the phosphate backbone and bases, respectively.

stem/loop I + stem/loop II (oligo II) of gND7-506 (Figure 3B) with apparent binding affinities (K_ds) of 7.0 ± 0.5 nM and 5.5 ± 0.9 nM, respectively, at salt concentrations of 50 mM NaCl. However, only weak binding was observed to the oligo(U)-tail ($K_d \sim 150$ nM) and essentially no binding to stem/loop I alone (Figure 3B). Because previous work suggested that ionic strength affects MRP-RNA binding, we measured MRP1/MRP2 binding to oligo II under conditions of increasing salt. The results reveal high affinity binding at physiologically relevant salt concentrations.

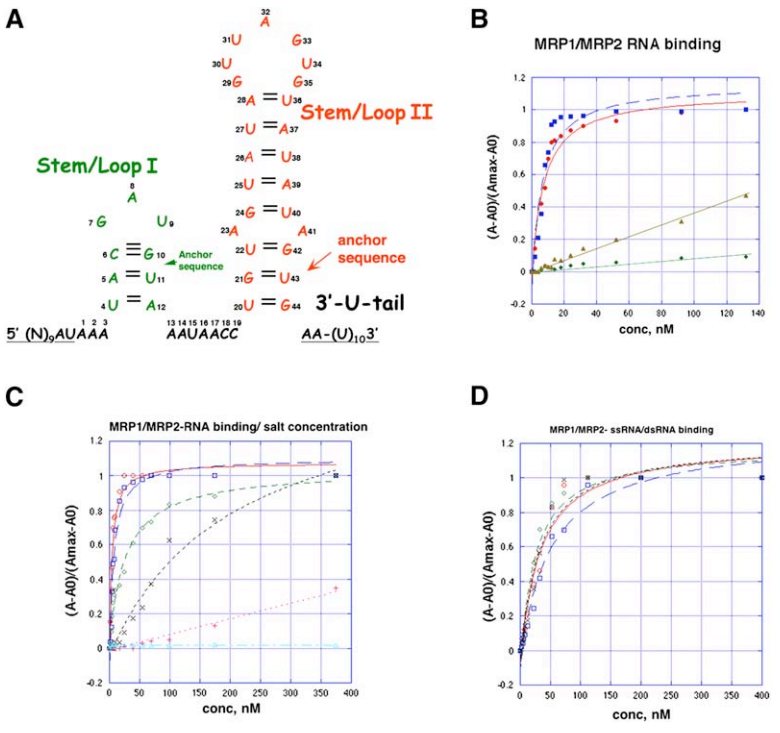

Figure 3. Characterization of MRP1/MRP2-RNA Interactions

(A) Schematic structure of the gRNA molecule gND7-506. Labeled are stem/loop I, stem/loop II, and the 3′ oligo(U) tail. Stem/loop I (anchor sequence) is colored green, stem/loop II is colored red, and the remaining nucleotides are shown in black. The base pairs encompassing the gRNA molecule used in cocrystallization with MRP1/MRP2 are numbered 1–44.

(B) FP studies of MRP1/MRP2 interaction with gRNA (gND7-506) fragments. Representative normalized, binding isotherms are shown. The resulting isotherms for MRP1/MRP2 interactions with the various RNAs are as follows: with stem/loop I-stem/loop II (nucleotides 4–44) (Figure 3A) (blue ■); stem/loop II (nucleotides 19–44) (red diamond), 3′ oligo(U) tail (AAUUUU UUUUUU) (yellow ▲), and stem/loop I alone (nucleotides 44–12) (green ◆). In this figure and Figures 3C and 3D, the concentration of protein (X axis) corresponds to MRP1/MRP2 dimer concentration.

(C) FP studies of MRP1/MRP2-gRNA (gND7-506) oligo II interaction under increasing salt concentrations. Normalized, binding isotherms are shown for NaCl concentrations of 50 mM (red ○), 100 mM (blue □), 150 mM (green ◇), 200 mM (black ×), 300 mM (pink +), and 400 mM (blue △).

(D) FP studies of MRP1/MRP2 interaction with ssRNA and dsRNA. Representative normalized, binding isotherms are shown for the given RNA molecules as follows: ssRNA, 27-mer A (red ○); ssRNA, GGUUAGG (blue □); dsRNA U/A 27-mer (green ◇) and dsRNA2 (black ×).

But at salt concentrations greater than 200 mM, binding is quickly abrogated (the K_ds were 5.1 ± 0.7 nM in 50 mM NaCl, 8.5 ± 1.4 nM in 100 mM NaCl, 27.1 ± 4.3 nM in 150 mM NaCl, 206 ± 50 nM in 200 mM NaCl, and no saturable binding in 300 and 400 mM NaCl) (Figure 3C). In addition, magnesium was not required for high-affinity binding (Figure S1).

We next found that MRP1/MRP2 bound two different ssRNAs with K_ds of 50.7 ± 11.0 nM and 32.6 ± 9.0 nM and two diverse dsRNAs with K_ds of 31.5 ± 9.2 nM and 24.2 ± 5.9 nM (Experimental Procedures; Figure 3D). Although these oligonucleotides did not bind as well as the gRNA molecule, the binding was high affinity and saturable. Indeed, these findings are consistent with the data from Aphasizhev et al. who showed that the *L. tarentolae* MRP1/MRP2 complex has no sequence specificity for RNA binding and little preference for ssRNA or dsRNA (Aphasizhev et al., 2003b). Like gRNA binding, the interaction of MRP1/MRP2 with these RNAs is dramatically affected by salt concentration and was completely abrogated in 200 mM NaCl (Figure S2). Because MRP1/MRP2 can bind in a nonsequence specific manner, it is notable that only weak binding was observed for the oligo(U) tail (Figure 3B). However, these data are consistent with previous studies, which also revealed no significant interaction between the MRPs and the oligo(U) tail (Hermann et al., 1997; Müller et al., 2001). Interestingly, long oligo(U) sequences can adopt several unusual higher-order structures, and such structures have been observed in gRNA oligo(U) tails (Lowman and Draper, 1986; Baeyens et al., 1995). To test whether RNA conformation affects MRP1/MRP2 binding, we analyzed MRP1/MRP2 binding to oligo(U) and stem/loop I RNA when unfolded and found that these unfolded RNAs bind with high affinities, similar to ssRNA and dsRNA (Figures S3A and S3B).

Thus, our binding data suggest that the MRP-RNA interaction is nonsequence specific, electrostatically driven, and affected by RNA structure. However, we also found that the MRP complex has a preference for gRNA (by 5- to10-fold). Indeed, if a primary function of MRP1/MRP2 is to bind gRNA and mediate gRNA-pre-mRNA matchmaking, such a preference would be necessary to prevent MRP sequestration by non-gRNAs in the mitochondrion.

Structure of an MRP1/MRP2-gRNA Complex

To understand how the MRP1/MRP2 complex can recognize multiple gRNA molecules in a nonsequence-specific manner, we determined the structure of an MRP1/MRP2-gRNA complex. Crystals of this complex were grown under low salt conditions using a gRNA fragment encompassing gND7-506 stem/loops I and II (gND7-506(I-II)), corresponding to nucleotides 1–44 in Figure 3A (Experimental Procedures). The structure was solved by Molecular Replacement and the ASU contains one MRP1, one MRP2, and one gND7-506(I–II). The heterotetramer, identical to that observed in our apo structures, is generated by crystallographic symmetry. The initial simulated annealing $2F_o - F_c$ composite omit map (calculated prior to inclusion of the RNA) revealed density for nucleotides 11–23 and 40–44 of the gRNA, which are bound via electrostatic interactions to the concave β sheet surface of both MRP1 and MRP2. The remaining nucleotides, which are apparently not bound by the MRPs, are disordered in the structure (Figures 4A, 4B, and 5A). The placement of the RNA was subsequently confirmed by a difference Fourier map utilizing data collected from a crystal in which U43 was replaced by 5-iodouracil (Experimental Procedures). Although the overall MRP1/MRP2 structure represents a new type of RNA binding fold, the MRP1/MRP2-gRNA structure shows that it has in common with several RNA binding proteins a curved β sheet surface, which serves as a binding site for extended RNA (Nagai, 1996). These regions of extended RNA include the base of stem/loop II of the gRNA and the anchor sequence, stem/loop I, which remarkably in the structure is bound in an unwound state with its bases exposed to the solvent (Figure 5A). Thus, the structure appears to have captured a critical step in the annealing reaction in which the anchor sequence is unfolded, in a form active for pre-mRNA annealing.

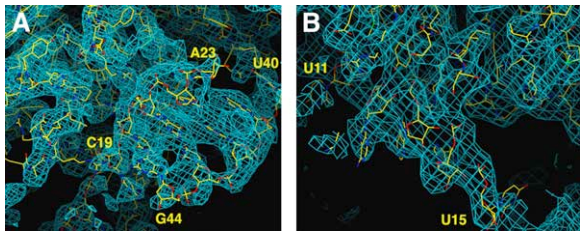

Figure 4. Initial Simulated Annealing $2F_o - F_c$ Electron Density Map for MRP1/MRP2-gRNA Complex

(A) A section of the initial $2F_o - F_c$ electron density map (3.37 Å) calculated before the RNA was added and contoured a 0.7 σ. Shown is the section of the map near MRP2. Density for the base of the stem/loop II is clearly visible, including density for nucleotides 19–23 and 40–44 (labeled).

(B) A section of the same initial simulated annealing $2F_o - F_c$ electron density map shown in Figure 4A highlighting the density near MRP1 and its bound anchor sequence. Labeled are nucleotides 11 and 15.

MRP1/MRP2 Bind gRNA via Nonsequence-Specific Electrostatic Interactions

Comparisons of the apoMRP1/MRP2 structures with the gRNA bound form revealed no large structural differences, indicating that gRNA binding does not alter the MRP1/MRP2 conformation. A key feature of the MRP1/MRP2-gRNA structure is the finding that the RNA is bound with its phosphate backbone anchored to the β sheet surface of the MRP proteins and its bases exposed. Indeed, the principal role played by charge-charge neutralization in this interaction is dramatically underscored by the electrostatic surface representation of MRP1/MRP2, which shows that the binding site for the gRNA is extremely electropositive, while the opposite face is highly electronegative (Figures 5B and 5C). Interestingly, there are no base stacking or base-specific interactions observed in the

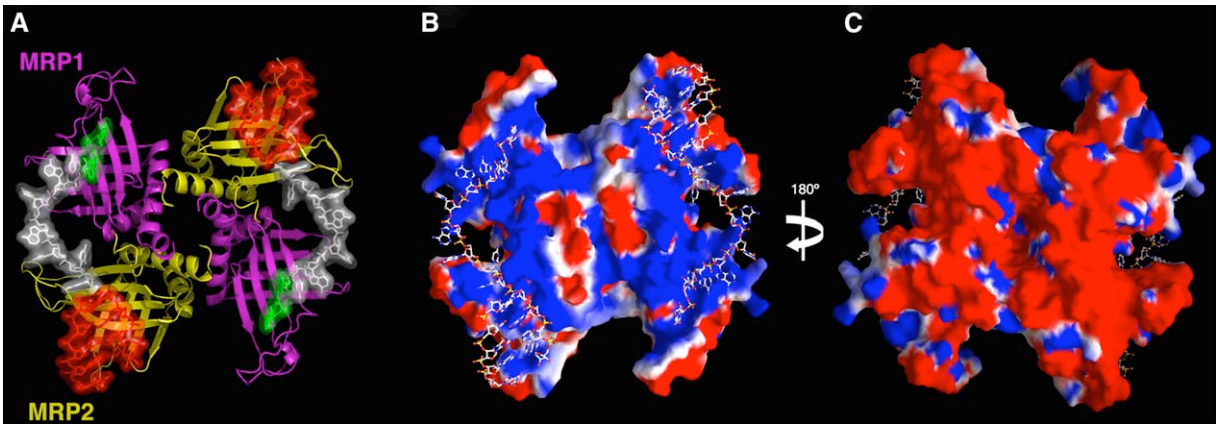

Figure 5. The Structure of a MRP1/MRP2-gND7-506 (I–II) Complex

(A) Ribbon diagram of the MRP1/MRP2-gND7-506 (I–II) complex. MRP1 and MRP2 are colored magenta and yellow. The RNA bases are color-coded as in Figure 3A and shown as transparent surfaces. Stem/loop I nucleotides are green, nucleotides between stem/loop I and II are white, and stem/loop II nucleotides are red.

(B) Electrostatic surface representation of the MRP1/MRP2 complex with the gRNA shown as sticks. Blue and red represent electropositive and electronegative surfaces, respectively. This figure and Figure 5C were made using GRASP (Nicholls et al., 1991).

(C) Electrostatic surface representation of the MRP1/MRP2-gRNA complex shown in Figure 5B rotated by 180°.

MRP1/MRP2-gRNA complex. This lack of specific interactions and the primary use of electrostatic-phosphate contacts explain the salt sensitivity and nonsequence specificity of MRP1/MRP2-RNA binding.

MRP1/MRP2-gRNA Interactions

In the MRP1/MRP2-gRNA structure there are three primary protein-RNA interaction modules; stem/loop II interacts with MRP2, the nucleotides between the anchor and stem/loop II interact with the basic region between MRP1 and MRP2, and the anchor sequence interacts with MRP1. The first interaction, between stem/loop II and MRP2, helps explain the ability of MRP1/MRP2 to bind dsRNA, as it reveals that the MRP complex can bind to the end of a dsRNA that is in an extended conformation. However, stem/loop II is primarily fastened to MRP2 via contacts to one of its strands, strand 1 (Figures 6A and 6B). The sole contact to strand 2 is from MRP2 residue Arg174, which makes electrostatic interactions with the Ade41 phosphate group and nonspecific base contacts with Ura40. Residues on the β sheet surface of MRP2 that bind strand 1 include Arg92, Arg96, His105, and Arg120 (Figure 6C). These residues make extensive interactions with the phosphate moieties of nucleotides 19–21, consistent with biochemical studies (Hermann et al., 1997) (Figures 6A and 6B). Finally, MRP2 residue Arg67 hydrogen bonds with the 2′ hydroxyl moiety of Cyt19 (Figure S4).

The second protein-RNA interaction module involves the RNA connecting the anchor-sequence region with stem/loop II region, nucleotides 15–18. These are the most disordered of the modeled nucleotides. However, they are tethered to the MRP complex by long-range electrostatic interactions, two nonspecific base contacts between MRP1 residue His90 to Cyt18 and between MRP2 residue Glu114 with Ade17 and an electrostatic interaction between Lys117 and the phosphate moiety of Ade17 (Figure 6D). The third MRP-RNA interaction module is comprised of contacts between MRP1 residues and nucleotides 11–14. Importantly, this bound RNA includes two nucleotides of the anchor sequence. In the folded gRNA, these nucleotides participate in two of the three base pairs that stabilize the stem. In the MRP1/MRP2-gRNA structure, these bound nucleotides are stabilized in the unfolded state. MRP1 residues Arg48, Tyr61, and Arg83 interact closely with the RNA phosphate backbone and favor binding of the two nucleotides of the anchor sequence in a single-stranded, extended conformation (Figures 6A and 6B). Arg83 also makes weak, nonspecific contacts to the adenine bases of Ade13 and Ade14 and Arg48 makes a weak contact to the 2′ hydroxyl moiety of Ura11. Finally, Ser85 and Arg87 make electrostatic interactions with the phosphate moiety of Ade13.

Studies showing that the gRNA stem/loops have low thermodynamic stability and require little energetic input for melting are consonant with the finding that the anchor sequence is unfolded when bound to the MRPs and also with the fact that the RNA at the top region of stem/loop II, nucleotides 25−40 (Figure 3A), are disordered in our structure. In fact, the 7 nucleotide loop at the top of gND7-506 stem/loop II is predicted to form a thermodynamically labile triple adenine tertiary interaction with the base of stem/loop I (Schmid et al., 1995; Hermann et al., 1997). Thus, unfolding of the anchor sequence would likely coincide with the unraveling of the tip of stem/loop II.

RNA Binding Stoichiometries: Insight into gRNA Binding Mechanism

As mentioned, MRP1 and MRP2 show a remarkable degree of structural homology with each other. In the MRP1/MRP2-RNA structure this homology is reflected in

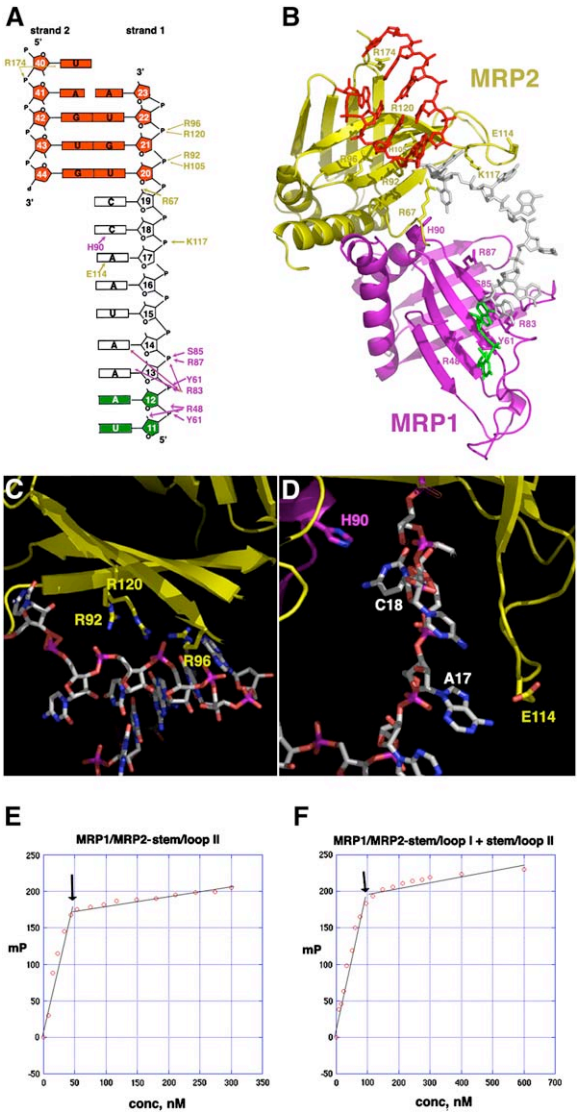

Figure 6. MRP1/MRP2-gRNA Interactions

(A) Schematic diagram of MRP1/MRP2-gND7-506 (I–II) contacts. Indicated are all electrostatic and direct contacts between gRNA and residues in the MRP1/MRP2 complex. The riboses of each nucleotide are numbered and shown as rectangles. Hydrogen bonds are indicated by arrows with contacts from MRP1 colored magenta and contacts from MRP2 colored yellow.

(B) Close-up view of the MRP1/MRP2-gND7-506 (I–II) interactions. MRP1 and MRP2 are colored magenta and yellow and the RNA is shown as sticks and colored as in Figure 3A. Residues that interact with the RNA are shown as sticks.

(C) Close-up view of the extensive phosphate interactions between stem/loop II nucleotides and MRP2.

(D) Close-up view of the two base contacts observed in the structure between His90 and Cyt18 and Glu114 and Ade17.

(E) Determination of the binding stoichiometry of the stem/loop II-MRP1/MRP2 interaction. Note the inflection point at an MRP1/MRP2 dimer concentration of 50 nM (black arrow) indicating the shift in high affinity to low affinity binding. This indicates that 4 stem/loop II molecules can bind a MRP1/MRP2 tetramer.

(F) Determination of the binding stoichiometry of the stem/loop I + II-MRP1/MRP2 interaction. Note the inflection point at an MRP1/MRP2 dimer concentration of 100 nM (black arrow) indicating that 2 stem/loop I + stem/loop II molecules can bind an MRP1/MRP2 tetramer.

the similar way that each of the MRP subunits interacts with RNA (Figure 5A). Combined with the fact that the MRPs bind RNA in a nonsequence-specific manner, this leads to the prediction that MRP1, which in the structure interacts with the anchor sequence should be able to bind stem/loop II and that MRP2, which binds stem/loop II, should be capable of interacting with the unfolded anchor sequence. If this prediction is correct, then oligo I, containing only stem/loop II, should be capable of interacting simultaneously with both MRP1 and MRP2. To test this hypothesis, we determined the binding stoichiometries of the MRP1/MRP2 complex for oligo I and the full-length gRNA mimic, stem/loop I + stem/loop II (oligo II) (Experimental Procedures). For this measurement, an FP assay was employed in which the concentration of the RNA molecules was increased to 100 nM, i.e., >10-fold higher that the K_d, thereby ensuring stoichiometric binding (Hoffmann et al., 2005). Our data reveal a 4:1 ratio of oligo I to MRP1/MRP2 tetramer, indicating that stem/loop II is indeed able to bind simultaneously and separately to both subunits of MRP1 and MRP2 (Figures 6E and 6F). By contrast, the ratio of oligo II to MRP1/MRP2 tetramer was 2:1, indicating that one full-length gRNA requires both MRP1 and MRP2 subunits for interaction, as observed in our structure.

It is notable that only one mode of binding is seen in the crystal structure, i.e., stem/loop II binds MRP2 and the anchor sequence binds MRP1. Analysis of the crystal packing of the protein molecules suggests that only this binding mode is observed because several packing interactions with protein residues near the bound anchor sequence would absolutely preclude binding of the double-stranded stem/loop II at this location. Specifically, these symmetry interactions would position MRP1 residues Arg150, Tyr151, Pro175, and Asp188 <1.0 Å from strand 2 nucleotides of stem/loop II (Figure S5).

Whirly-DNA versus Whirly-RNA Binding

The primary use of electrostatic complementation explains how the MRPs can bind RNA molecules in a nonsequence-specific manner. However, this binding mode is likely different from that utilized by p24, which binds ssDNA in a sequence-specific manner (Desveaux et al., 2002). Structure-based sequence comparisons of the MRPs with p24 show that the residues that contact RNA in the MRP1/MRP2-gRNA complex are not conserved in p24. Although the same face of the β sheet surface of p24 is predicted to bind ssDNA, the residues on this surface are primarily aromatic and hydrophobic compared to the abundance of arginine residues observed in the MRPs. A KGKAAL motif, located on β2, is conserved in the Whirly plant family and is predicted to be a central ssDNA binding determinant. This motif, however, is completely absent in both MRP1 and MRP2. Thus, although

there may be similarities in the MRP-gRNA and p24-ssDNA interactions in that both likely bind extended polynucleotides on the same surface, it appears these proteins have evolved to bind nucleotides differently.

The MRPs May Play Roles in Multiple RNA Processes

The ability of the MRPs to bind RNA in a sequence-nonspecific manner strongly suggests that these proteins could be involved in other RNA processes. In fact, the results obtained from cells with downregulated MRPs indicate that, in addition to gRNA-pre-mRNA annealing, the MRPs might be involved in RNA turnover and polycistronic pre-mRNA processing or they may have transcript-specific roles (Vondrušková et al., 2005). This would not be unprecedented as other RNA binding proteins function in multiple RNA processes, such as the Ro autoantigen, which binds misfolded RNAs and functions in RNA quality control as well as binding small RNAs termed Y RNAs (Chen and Wolin, 2004). The structure of Ro, which consists of a von Willebrand factor A domain and a HEAT repeat domain, bound to RNA was recently determined and revealed several RNA binding sites on the Ro complex (Stein et al., 2005). This is reminiscent of the multiple binding pockets revealed in the MRP structure. Although Ro is a sequence specific RNA binding protein, it binds double stranded Y RNA in a crevice on the exterior of its protein ring similar to how MRP1/MRP2 binds stem/loop II. However, whether MRP1/MRP2, like Ro, plays multiple roles in RNA processes remains to be determined.

Mechanism of gRNA-pre-mRNA Annealing Revealed in the MRP1/MRP2-gRNA Structure

Pivotal studies by the Göringer and Simpson laboratories demonstrated that the *T. brucei* and *L. tarentolae* MRP proteins act as molecular matchmakers by promoting the annealing of gRNAs with cognate pre-mRNAs (Müller et al., 2001; Aphasizhev et al., 2003b). These studies suggested that the MRPs act on the basis of two mechanistic principles. First, MRP binding to the gRNA converts the RNA to an annealing-active conformation. Second, the MRP proteins decrease the electrostatic repulsion between the two RNA substrates, favoring the formation of the gRNA-pre-mRNA hybrid. Remarkably, two separate gRNA binding determinants were proposed for MRP; a binding pocket for stem/loop II and a so-called ''presentation platform'' for the anchor sequence (Müller et al., 2001). These data and the resulting mechanistic predictions can now be readily explained by the structure of the MRP1/MRP2-gRNA complex. The structure reveals that stem/loop II and the anchor sequence are indeed both bound by two separate platforms. In the structure, the base of stem/loop II is bound by one site (MRP2), while the anchor sequence is bound by a second binding platform (MRP1). Our biochemical data indicate that stem/loop II likely binds first in the reaction. The MRP1/MRP2-stem/loop II interaction would then disrupt the stem/loop I-stem/loop II triple adenine interaction, tethering the thermodynamically labile anchor sequence (stem/loop I) near the second binding platform. Unfolding of stem/loop I would then produce an extended RNA conformation that can be readily bound by MRP1/MRP2, as confirmed by our biochemical studies. Thus, the end result of MRP1/MRP2-gRNA binding is the presentation of the anchor sequence in an unfolded state with the bases exposed to the solvent in a conformation suitable for hybridization with cognate pre-mRNA. Thus, the MRP1/MRP2-gRNA structure provides an atomic level description of a general mechanism for protein-assisted RNA duplex formation.

EXPERIMENTAL PROCEDURES

Preparation of the Coexpression System, Crystallization, and Structure Determination of apoMRP1/MRP2 Complexes

The MRP1/MRP2 coexpression system was constructed by subcloning the MRP1 gene-fragment encoding residues 20–176 (which removed the N-terminal mito-targeting sequence and a C-terminal region found to cause insolubility) and the MRP2 gene-fragment encoding residues 30–224 (which removed the N-terminal mito-targeting sequence) into the pETDuet-1 coexpression vector. Crystals were obtained by mixing purified MRP1/MRP2 (25–30 mg/ml) 1:1 with the reservoir of 0.17 M ammonium acetate, 0.08 M sodium acetate pH 4.6, 25.5% PEG 4000, and 15% glycerol. The crystals are monoclinic, space group $P2_1$, with a = 60.3 Å, b = 85.7 Å, c = 86.9 Å, and b = 109.4°. MAD X-ray intensity data were collected from a crystal soaked for a week in methyl mercuric acetate (Table 1). All data were processed with MOSFLM. MAD phasing followed by Density Modification in CNS produced a clearly interpretable map (Brünger et al., 1998; Terwilliger and Berendzen, 1999). The model was refined against a native 1.89 Å resolution data set to a final R_{free} of 21.7% (Jones et al., 1991; Brünger et al., 1998) and includes residues 28–173 of both MRP1 subunits, residues 55–175 and 188–221 of one MRP2 subunit, residues 56–175 and 188–221 of the second MRP2 subunit, 8 acetate molecules, and 572 water molecules. The model has excellent stereochemistry with 90.9% of residues in most favored regions of the Ramachandran plot, 8.7% in additionally allowed, 0.4% in generously allowed, and 0 in the disallowed region (Laskowski et al., 1993).

A second, rhombohedral, crystal form of apoMRP1/MRP2 was obtained (Table 1), solved by Molecular Replacement using EPMR (Kissinger et al., 1999), and was minimally refined to an R_{free} of 29.9% to 3.35 Å resolution. The model contains two tetramers that are identical to the $P2_1$ tetramer structure and consists of residues 28–173 of each of the four MRP1 subunits, 60–175 and 188–221 of one MRP2 subunit and 59–175 and 188–221 of three of the MRP2 subunits and 56 solvent molecules.

Characterization of the MRP1/MRP2-RNA Interaction with FP

Fluorescence Polarization (FP) measurements were collected with a PanVera Beacon 2000 Fluorescence Polarization System at 27°C. Samples were excited at 490 nM and fluorescence emission was measured at 520 nM. For gRNA binding studies, FP experiments were carried out with 5′-fluorescinated oligos that included stem/loop I (nucleotides 4–12) (oligo I), stem/loop II (nucleotides 19–44), the 3′ oligo(U) tail (AAUUUUUUUUU) and stem/loop I-stem/loop II (nucleotides 4–44) (oligo II) (Figure 3A). For each experiment, MRP1/MRP2 complex was titrated into a 0.990 ml reaction buffer (25 mM Tris pH 7.5, 50 mM NaCl) containing 1 nM fluorescinated RNA fragment. To test binding of the unfolded oligo(U) tail and stem/loop I RNA, the oligos (1 uM stock concentrations) were heated to 100°C and added directly to the 0.990 ml reaction buffer at a final concentration of 1 nM and the measurements taken immediately at 27°C. All FP data were fit to a simple bimolecular binding model by nonlinear regression and the concentration of MRP1/MRP2 used to fit the data is for an MRP1/MRP2 ''dimer.'' For salt studies, the same buffer was utilized except that the salt varied

(50 mM, 100 mM, 150 mM, 200 mM, 300 mM, and 400 mM) and fluorescinated oligo II was used. To test binding of ssRNA and dsRNAs to MRP1/MRP2, two fluorescinated ssRNA molecules (5′-GGUUAGG-3′ and a 27-mer containing all adenines) and two fluorescinated dsRNAs (5′-ACUGAC-3′ annealed with 5′-GUCAGU-3′ and a 27-mer A-U duplex) were used.

To determine the stoichiometries of MRP1/MRP2 binding to oligos I and II, the high affinity buffer, i.e., 25 mM Tris pH 7.5, 50 mM NaCl was used, and the concentration of the RNA molecules was increased to 100 nM, i.e., >10-fold higher than the K_d, to ensure stoichiometric binding. In this case, the titration of the MRP1/MRP2 complex into the solution results in a linear increase in the observed millipolarization (mP) until the high-affinity RNA sites are saturated. Following saturation, the plot plateaus in a roughly flat line, indicative of no binding or low-affinity binding. The inflection point, which occurs at the intersection of the two lines, reveals the concentration of the MRP1/MRP2 dimer required for saturation.

Crystallization and Structure Determination: MRP1/MRP2-gRNA Complex

For crystallization trials, several gRNA molecules that contained stem/loop II or stem/loops I and II were tried. Crystals were obtained using a 44-mer gRNA molecule corresponding to gND7-506 nucleotides 1–44 (Figure 3A), in which the 3′ most guanine was a deoxyoligonucleotide to facilitate synthesis of the long RNA. MRP1/MRP2 was mixed in various ratios with the 44-mer gND7-506 gRNA. Crystals were obtained using the hanging drop vapor diffusion method by mixing the MRP1/MRP2-gRNA complex 1:2 with the reservoir of 20% PEG 4000, 10% isopropanol, and 0.1 M HEPES pH 7.5, which contains no salt. The crystals were hexagonal, $P6_122$, with a = b = 157.6 Å, and c = 81.3 Å, and they contain one MRP1 subunit, one MRP2 subunit and one gRNA in the ASU. The heterotetramer is generated by crystallographic symmetry and is identical to the apoMRP1/MRP2 heterotetramer. The crystals were extremely labile and lost diffraction completely within 3 days after they appeared, and the diffraction was highly mosaic >2.0°. However, the structure was readily solved (with data collected at ALS beamline 8.3.1) using the program EPMR (Kissinger et al., 1999). Following initial refinement, the $2F_o-F_c$ simulated annealing map (Figures 4A and 4B) revealed density for nucleotides 11–23 and 40–44. The structure was minimally refined in CNS to a final R_{free} of 29.9% to 3.37 Å resolution. Subsequently, a 3.5 Å resolution data set was collected from a crystal in which U43 was replaced by 5-iodouracil. A difference Fourier map calculated with these data, which revealed a peak for the iodine atom, confirmed the position of the RNA. The model consists of residues 27–173 of the MRP1 subunit, 65–175 and 188–221 of the MRP2 subunit, and nucleotides 11–23 and 40–44 of the gND7-506 gRNA molecule (Figure 3A).

Supplemental Data

Supplemental Data include five figures and can be found with this article online at http://www.cell.com/cgi/content/full/126/4/■■■/DC1/.

ACKNOWLEDGMENTS

This work was supported by the Burroughs Wellcome Career Development Award 992863 and MD Anderson Research Trust Fellowship (to M.A.S), National Institutes of Health grant 5R03TW6445 (to Ken Stuart and J.L.), and Grant Agency of the Czech Republic grant P191/2004 (to L.T.). Coordinates for the apoMRP1/MRP2 and the MRP1/MRP2-gRNA complexes have been deposited with the Protein Data Bank under the Accession codes 2GIA, 2GID, and 2GJE, respectively.

Received: April 3, 2006
Revised: May 19, 2006
Accepted: June 23, 2006
Published: August 24, 2006

REFERENCES

Aphasizhev, R., Aphasizhev, I., Nelson, R.E., Gao, G.H., Simpson, A.M., Kang, X.D., Falick, A.M., Sbicego, S., and Simpson, L. (2003a). Isolation of a U-insertion/deletion editing complex from *Leishmania tarentolae* mitochondria. EMBO J. *22*, 913–924.

Aphasizhev, R., Aphasizheva, I., Nelson, R.E., and Simpson, L. (2003b). A 100-kD complex of two RNA-binding proteins from mitochondria of *Leishmania tarentolae* catalyzes RNA annealing and interacts with several RNA editing components. RNA *9*, 62–76.

Baeyens, K.J., De Bondt, H.L., and Holbrook, S.R. (1995). Structure of an RNA double helix including uracil-uracil base pairs in an internal loop. Nat. Struct. Biol. *2*, 56–61.

Benne, R., Van den Burg, J., Brakenhoff, J.P., Sloof, P., Van Bloom, J.H., and Tromp, M.C. (1986). Major transcript of the frameshifted coxII gene from trypanosome mitochondria contains four nucleotides that are not encoded in the DNA. Cell *46*, 819–826.

Blom, D., Van den Burg, J., Breek, C.K., Speijer, D., Muijsers, A.O., and Benne, R. (2001). Cloning and characterization of two guide RNA-binding proteins from mitochondria of *Crithidia fasciculata*: gBP27, a novel protein, and gBP29, the orthologue of *Trypanosoma brucei* gBP21. Nucleic Acids Res. *29*, 2950–2962.

Blum, B., and Simpson, L. (1990). Guide RNAs in kinetoplastid mitochondria have a nonencoded 3′ oligo(U) tail involved in recognition of the preedited region. Cell *62*, 391–397.

Blum, B., Bakalara, N., and Simpson, L. (1990). A model for RNA editing in kinetoplastid mitochondria: guide RNA molecules transcribed from maxicircle DNA provide the edited information. Cell *60*, 189–198.

Brünger, A.T., Adams, P.D., Clore, G.M., DeLano, W.L., Gros, P., Crosse-Kunstleve, R.W., Jiang, J.S., Kuszewski, J., Nilges, M., Pannu, N.S., et al. (1998). Crystallography and NMR System: A new software suite for macromolecular structure determination. Acta Crystallogr. D Biol. Crystallogr. *54*, 905–921.

Chen, X., and Wolin, S.L. (2004). The Ro 60 kDa autoantigen: insights into cellular function and role in autoimmunity. J. Mol. Med. *84*, 232–239.

Corell, R.A., Feagin, J.E., Riley, G.R., Strickland, T., Guderian, J.A., Myler, P.J., and Stuart, K. (1993). *Trypanosoma brucei* minicircles encode multiple guide RNAs which can direct editing of extensively overlapping sequences. Nucleic Acids Res. *21*, 4313–4320.

Corell, R.A., Read, L.K., Riley, G.R., Nellissery, J.K., Allen, T.E., Kable, M.L., Wachal, M.D., Seiwert, S.D., Myler, P.J., and Stuart, K. (1996). Complexes from *Trypanosoma brucei* that exhibit deletion editing and other editing-associated properties. Mol. Cell. Biol. *16*, 1410–1418.

Delano, W.L. (2002). The PyMOL Molecular Graphics System (San Carlos, CA: DeLano Scientific).

Desveaux, D., Allard, J., Brisson, N., and Sygusch, J. (2002). A new family of plant transcription factors displays a novel ssDNA-binding surface. Nat. Struct. Biol. *9*, 512–517.

Feagin, J.E., Shaw, J.M., Simpson, L., and Stuart, K. (1988a). Creation of AUG initiation codons by addition of uridines within cytochrome b transcripts of kinetoplastids. Proc. Natl. Acad. Sci. USA *85*, 539–543.

Feagin, J.E., Abraham, J.M., and Stuart, K. (1988b). Extensive editing of the cytochrome c oxidase III transcript in *Trypanosoma brucei*. Cell *53*, 413–422.

Hermann, T., Schmid, B., Heumann, H., and Göringer, H.U. (1997). A three-dimensional working model for a guide RNA from *Trypanosoma brucei*. Nucleic Acids Res. *25*, 2311–2318.

Hoffmann, K.M., Williams, D., Shafer, W.M., and Brennan, R.G. (2005). Characterization of the multiple transferable resistance repressor, MtrR, from *Neisseria gonorrhoeae*. J. Bacteriol. *187*, 5008–5012.

Holm, L., and Sander, C. (1995). Dali: a network tool for protein structure comparison. Trends Biochem. Sci. *20*, 478–480.

Hong, M., and Simpson, L. (2003). Genomic organization of Trypanosoma brucei kinetoplast DNA minicircles. Protist *154*, 265–279.

Horváth, A., Berry, E.A., and Maslov, D.A. (2000). Translation of the edited mRNA for cytochrome b in trypanosome mitochondria. Science *287*, 1639–1640.

Jones, T.A., Zou, J.-Y., Cowan, S.W., and Kjeldgaard, M. (1991). Improved methods for building protein models in electron density maps and the location of errors in these models. Acta Crystallogr. *A47*, 110–119.

Kissinger, C.R., Gehlhaar, D.K., and Fogel, D.B. (1999). Rapid automated molecular replacement by evolutionary search. Acta Crystallogr. D Biol. Crystallogr. *55*, 484–491.

Köller, J., Müller, U.F., Schmid, B., Missel, A., Kruft, V., Stuart, K., and Göringer, H.U. (1997). *Trypanosoma brucei* gBP21. An arginine-rich mitochondrial protein that binds to guide RNA with high affinity. J. Biol. Chem. *272*, 3749–3757.

Koslowsky, D.J., Riley, G.R., Feagin, J.E., and Stuart, K. (1992). Guide RNAs for transcripts with developmentally regulated RNA editing are present in both life cycle stages of *Trypanosoma brucei*. Mol. Cell. Biol. *12*, 2043–2049.

Krause, K., Kilbienski, I., Mulisch, M., Rodiger, A., Schafer, A., and Krupinska, K. (2005). DNA-binding proteins of the Whirly family in *Arabidopsis thaliana* are targeted to the organelles. FEBS Lett. *579*, 3707–3712.

Lambert, L., Müller, U.F., Souza, A.E., and Göringer, H.U. (1999). The involvement of gRNA-binding protein gBP21 in RNA editing- an *in vitro* and *in vivo* analysis. Nucleic Acids Res. *27*, 1429–1436.

Laskowski, R.A., MacArthur, M.W., Moss, D.S., and Thornton, J.M. (1993). PROCHECK: a program to check the stereochemical quality of protein structures. J. Appl. Crystallogr. *26*, 283–291.

Liu, Y., Motyka, S.A., and Englund, P.T. (2005). Effects of RNA interference of Trypanosoma brucei structure-specific endonuclease-I on kinetoplastid DNA replication. J. Biol. Chem. *280*, 35513–35520.

Lowman, H.B., and Draper, D.E. (1986). On the recognition of helical RNA by cobra venom V1 nuclease. J. Biol. Chem. *261*, 5396–5403.

Lukeš, J., Hashimi, H., and Zíková, A. (2005). Unexplained complexity of the mitochondrial genome and transcriptome in kinetoplastid flagellates. Curr. Genet. *48*, 277–299.

Madison-Antenucci, S., and Hajduk, S.L. (2002). Editing machines: The complexities of trypanosome RNA editing. Cell *108*, 435–438.

Maslov, D.A., and Simpson, L. (1992). The polarity of editing within a multiple gRNA-mediated domain is due to formation of anchors for upstream gRNAs by downstream editing. Cell *70*, 459–467.

Müller, U.F., and Göringer, H.U. (2002). Mechanism of the gBP21-mediated RNA/RNA annealing reaction: matchmaking and charge reduction. Nucleic Acids Res. *30*, 447–455.

Müller, U.F., Lambert, L., and Göringer, H.U. (2001). Annealing of RNA editing substrates facilitated by guide RNA-binding protein gBP21. EMBO J. *20*, 1394–1404.

Nagai, K. (1996). RNA-protein complexes. Curr. Opin. Struct. Biol. *6*, 53–61.

Nicholls, A., Sharp, K.A., and Honig, B. (1991). Protein folding and association: insights from the interfacial and thermodynamic properties of hydrocarbons. Proteins *11*, 281–296.

Panigrahi, A.K., Schnaufer, A., Carmean, N., Igo, R.P., Gygi, S.P., Ernst, N.L., Palazzo, S.S., Weston, D.S., Abersold, R., Salavati, R., and Stuart, K. (2001). Four related proteins of the *Trypanosoma brucei* RNA editing complex. Mol. Cell. Biol. *21*, 6833–6840.

Panigrahi, A.K., Schnaufer, A., Ernst, N.L., Wang, B., Carmean, N., Salavati, R., and Stuart, K. (2003). Identification of novel components of *Trypanosoma brucei* editosomes. RNA *9*, 484–492.

Schmid, B., Riley, G.R., Stuart, K., and Göringer, H.U. (1995). The secondary structure of guide RNA molecules from *Trypanosoma brucei*. Nucleic Acids Res. *23*, 3093–3102.

Seiwert, S.D., and Stuart, K. (1994). RNA editing: transfer of genetic information from gRNA to precursor mRNA *in vitro*. Science *266*, 114–117.

Seiwert, S.D., Heidemann, S., and Stuart, K. (1996). Direct visualization of uridylate deletion *in vitro* suggests a mechanism for kinetoplastid RNA editing. Cell *84*, 831–841.

Shaw, J.M., Feagin, J.E., Stuart, K., and Simpson, L. (1988). Editing of kinteoplastid mitochondrial mRNAs by uridine addition and deletion generates conserved amino acid sequences and AUG initiation codons. Cell *53*, 401–411.

Simpson, A.G.B., Stevens, J.R., and Lukeš, J. (2006). The evolution and diversity of kinetoplastid flagellates. Trends Parasitol., in press.

Simpson, L., Sbicego, S., and Aphasizhev, R. (2003). Uridine insertion/deletion RNA editing in trypanosome mitochondria: a complex business. RNA *9*, 265–276.

Simpson, L., Aphasizhev, R., Gao, G., and Kang, X. (2004). Mitochondrial proteins and complexes in *Leishmania* and *Trypanosoma* involved in U insertion/deletion RNA editing. RNA *10*, 159–170.

Stein, A.J., Fuchs, G., Fu, C., Wolin, S.L., and Reinisch, K.M. (2005). Structural insights into RNA quality control: the Ro autoantigen binds misfolded RNAs via its central cavity. Cell *121*, 529–539.

Stuart, K.D., Schnaufer, A., Ernst, N.L., and Panigrahi, A.K. (2005). Complex management: RNA editing in trypanosomes. Trends Biochem. Sci. *30*, 97–105.

Sturm, N.R., and Simpson, L. (1990). Kinetoplast DNA minicircles encode guide RNAs for editing of cytochrome oxidase subunit III mRNA. Cell *61*, 879–884.

Terwilliger, T.C., and Berendzen, J. (1999). Automated MAD and MIR structure solution. Acta Crystallogr. D Biol. Crystallogr. *55*, 849–861.

Vondrušková, E., van den Burg, J., Zíková, A., Ernst, N.L., Stuart, K., Benne, R., and Lukeš, J. (2005). RNA interference analyses suggest a transcript-specific regulatory role for mitochondrial RNA-binding proteins MRP1 and MRP2 in RNA editing and other RNA processing in *Trypanosoma brucei*. J. Biol. Chem. *280*, 2429–2438.

Accession Numbers

Coordinates for the apoMRP1/MRP2 and the MRP1/MRP2-gRNA complexes have been deposited with the Protein Data Bank under the Accession codes 2GIA, 2GID, and 2GJE, respectively.